First-principles elastic and thermal properties of TiO_2: a phonon approach

2010 J. Phys.: Condens. Matter 22 015401

(http://iopscience.iop.org/0953-8984/22/1/015401)

IOP Publishing Journal of Physics: Condensed Matter

J. Phys.: Condens. Matter **22** (2010) 015401 (8pp) doi:10.1088/0953-8984/22/1/015401

First-principles elastic and thermal properties of TiO_2: a phonon approach

E Shojaee[1] **and M R Mohammadizadeh**[1,2,3]

[1] Superconductivity Research Laboratory (SRL), Department of Physics, University of Tehran, North Karegar Avenue, PO Box 14395-547, Tehran, Iran
[2] Computational Physical Sciences Laboratory, Department of Nano-Science, Institute for Research in Fundamental Sciences (IPM), PO Box 19395-5531, Tehran, Iran

E-mail: zadeh@ut.ac.ir and mohammadi@nano.ipm.ac.ir

Received 4 August 2009, in final form 4 November 2009
Published 2 December 2009
Online at stacks.iop.org/JPhysCM/22/015401

Abstract

Elastic and thermal properties of the TiO_2 lattice in anatase and rutile phases were studied in the framework of density functional perturbation theory within the local density approximation (LDA) and generalized-gradient approximation (GGA). The full elastic constant tensors of the polymorphs were calculated by linear fits to the acoustic branches of the phonon band structure near the center of the first Brillouin zone in symmetry directions of the crystals. It was observed that the elastic constants within the GGA are in better agreement with experiment. In addition, the Born effective charges, dielectric tensor, heat capacity, mean sound velocity and Debye temperature were calculated. The heat capacity at room temperature and the Debye temperature within the LDA are in better agreement with the experimental results. Therefore, using the phonon band structure and the density of states, one can obtain the important mechanical and thermal properties of materials.

(Some figures in this article are in colour only in the electronic version)

1. Introduction

Elastic constants as important factors of crystals characterize their response to the external forces. Calculation of these constants can play an important role in determining the specifications of new proposed materials in order to improve their performance in various applications. Among many experimental techniques to measure the elastic constants of crystals, ultrasonic measurements [1] and Brillouin spectroscopy [2] are the most common methods, due to their applicability to a wide variety of physical environments. Apart from the experimental work, recently some efforts have been focused on calculating the elastic constants of materials by first-principles calculations. The common way for this is to fit a line to the calculated stress as a function of strain [3].

Titanium dioxide has been of great interest in recent decades due to its interesting properties like superhydrophilicity and photocatalytic features [4]. The structural, electronic and optical properties of naturally grown polymorphs of titanium dioxide, anatase ($I_{4_1}amd$), rutile ($P4_2/mnm$) and brookite ($Pbca$), and its synthesized cotunnite (orthorhombic structure) and fluorite (cubic structure) phases (which are among the least compressible polycrystalline metal oxides reported) have already been studied in numerous works and approaches [5]. Among these studies, density functional theory and Kohn–Sham equations played a special role, with attention to their successes and failures [6]. More accurate studies beyond the mean-field theories [7] have been performed, e.g. Anisimov *et al* [8] and Wang and Doren [9] have studied rutile and anatase electronic structures, respectively, within the LDA + U which incorporates the strongly correlated interactions of 3d electrons of Ti. They have shown that the energy bandgap of these polymorphs can be obtained with good accuracy by this approach. The self-interaction correction scheme has the same effect [10].

The earliest major works on lattice dynamics of the rutile phase have been published by Lee *et al* [11, 12]. Their attention was on dielectric properties and phonon frequencies at the gamma point of the rutile structure in the framework of variational density functional perturbation theory (DFPT). The effect of (PW91) in structural properties and zone-center

[3] Address for correspondence: Superconductivity Research Laboratory (SRL), Department of Physics, University of Tehran, North Karegar Avenue, PO Box 14395-547, Tehran, Iran.

phonon frequencies in the rutile phase has been reported by Montanari and Harrison, too [13]. They have used LDA [14] and two kinds of GGAs, PBE [15] and PW91 [16], in exchange–correlation energy calculations. According to their results, PBE predicts the frequency of the transverse optical (TO) A_{2u} mode to be imaginary, leading to instability and to a ferroelectric phase transition which disagrees with all previous findings [13]. The phonon band structure and density of states of the rutile structure have also been reported using the straight supercell method by Sikora [17]. The major work for the anatase phase has been performed by Mikami *et al* [18]. They have investigated the dielectric properties, gamma point frequencies (including LO–TO splitting) and the phonon band structure in the pseudopotential DFPT approach.

The elastic constants of CeO_2, which have been calculated within the LDA [19], are in better agreement with experiment than in LDA + U [20]. The structural parameters like lattice parameters, bulk modulus and pressure derivative of the bulk modulus within LDA and LDA + U have almost the same accuracy with respect to the experimental data [20]. The acoustic modes of NiO have been well predicted by the LSDA approach, as well [21]. In three Raman-active A_g modes of the TiOCl system, the LDA + U result for one of the modes, and LDA results for the other two, are in better agreement with the experimental results [22]. For phonon frequencies and structural parameters of $BiFeO_3$, the GGA functional appears as the most reliable approximation even in comparison to the LDA + U [23]. Therefore, the error in the calculated vibrational and structural properties within the LDA + U is almost like the LDA and GGA results. So, one can use the LDA and GGA instead of the LDA + U approach concerning the dynamical properties of materials as well.

The main goal of this work is to determine the elastic constants of the anatase and rutile phases in a phonon approach. So we have studied the lattice dynamics of rutile and anatase polymorphs including dielectric properties, phonon band structure and density of states in the framework of DFPT, using both LDA and GGA. As a consequence the heat capacity and Debye temperature in the polymorphs were presented. In addition, we obtained elastic constants of them using our calculated phonon band structure. This method is not a simple way to estimate the elastic constants, but it has several advantages such as a criterion to investigate the accuracy of acoustic branches in the phonon dispersion curve, which is the challenging part of the phonon band structure. Investigation of the highest optical branch of graphene has recently been used to show the failure of density functional theory [24].

2. Computational details

The present results were obtained using the Q-Espresso package [25]. The calculations were performed in the framework of DFPT [26–28] using pseudopotentials and a plane-wave basis set. The calculated relaxed lattice structural parameters used in the phonon calculations are presented in table 1. As a usual result, LDA underestimates and GGA overestimates the equilibrium lattice parameters and volume [30].

Table 1. The relaxed lattice parameters within the LDA and PW91 calculations compared with the experimental values. u is the internal parameter for the position of atoms.

	a (au)	c/a	u
Anatase (LDA)	7.053	2.5197	0.2087
Anatase (PW91)	7.167	2.5584	0.2064
Exp.[a]	7.153	2.5135	0.2081
Rutile (LDA)	8.570	0.6414	0.3029
Rutile (PW91)	8.763	0.6383	0.3052
Exp.[a]	8.681	0.6442	0.3048

[a] Reference [29].

The Perdew–Zunger [14] ultrasoft [31] pseudopotentials were used for titanium and oxygen atoms in the LDA and Perdew–Wang [16] ultrasoft pseudopotentials in the GGA (PW91). In the titanium (oxygen) pseudopotential, 3s, 3p, 4s and 3d (2s and 2p) electrons were considered as the valence electrons. The cutoff energies for the plane-wave basis set in the wavefunction and in the charge density were 33 and 462 Ryd, respectively. The Brillouin zone (BZ) integration was performed with k points in the Monkhorst–Pack [32] (4, 4, 4) grid with the 11(6) reduced number of k points in the irreducible edge of the first BZ for the anatase (rutile) phase. We have also checked more dense grids, but the results did not change considerably. So, the mesh used is sufficient as it has already been used in these structures [18, 33].

Dynamical properties of these polymorphs were studied in the framework of DFPT which allows the use of only the unit cell to calculate phonons of any wavevector. The phonon frequencies were obtained by diagonalizing the dynamical matrix (DM) associated with any wavevector q in the first BZ. The DM elements were also found by solving self-consistent coupled equations of the variation of potential and the linear response of electronic density [26].

In order to obtain the phonon dispersion curve, the DM elements were calculated for q vectors in the Monkhorst–Pack method (4, 4, 4) grid sampling with a shift to contain the gamma point, reduced to 13(18) k points in the irreducible edge of the first BZ for the anatase (rutile) structure. Then, the inter-atomic force constants were obtained using Fourier transformation.

Anatase and rutile phases are in tetragonal crystal classes. So, the non-zero elastic constants are C_{11}, C_{12}, C_{13}, C_{33}, C_{44} and C_{66}. Attending the linear behavior of the acoustic branches near the zone center, one can obtain these constants by the descents of the mentioned lines. In more detail, if someone plots the phonon frequencies of the acoustic branches versus k points in the symmetry directions of the first BZ, and fits lines to their linear part (which is near the zone center), the slopes of these lines are equal to the velocities of the sound propagating in the noted directions. Then, we are able to calculate the elastic constants. For crystal classes including anatase and rutile structures, C_{11} is obtained from the quasilongitudinal mode in the [100] direction, C_{44} from the degenerated mode in the [001] direction, C_{66} from the quasishear mode in the [100] direction, C_{33} from the quasilongitudinal mode in the [001] direction, C_{12} from the quasishear mode in the [110] direction

Table 2. Anatase dielectric tensor elements, compared with the other results.

Anatase	This work (LDA)	This work (PW91)	Theory[a]	Exp.[b]
$\varepsilon_{xx} = \varepsilon_{yy}$	7.16	7.10	7.07	6.55
ε_{zz}	6.24	6.29	6.21	6.20

[a] Reference [18]. [b] Reference [35].

Table 3. Rutile dielectric tensor elements, compared with the other results.

Rutile	This work (LDA)	This work (PW91)	Theory[a]	Exp.[b]
$\varepsilon_{xx} = \varepsilon_{yy}$	7.56	7.39	7.54	6.84
ε_{zz}	8.26	8.40	8.67	8.43

[a] Reference [12]. [b] Reference [35].

and finally C_{13} from the quasishear mode in the [101] direction of the crystals [34]:

$$v_{ql}[100] = \sqrt{\frac{C_{11}}{\rho}}, \qquad v_{\text{degenerated}}[001] = \sqrt{\frac{C_{44}}{\rho}},$$

$$v_{qs}[100] = \sqrt{\frac{C_{66}}{\rho}} \qquad v_{ql}[001] = \sqrt{\frac{C_{33}}{\rho}},$$

$$v_{qs}[110] = \sqrt{\frac{C_{11} - C_{12}}{2\rho}},$$

$$v_{qs}[101] = \sqrt{\frac{C_{11}+C_{33}+2C_{44}-\sqrt{(C_{11}-C_{33})^2+4(C_{13}+C_{44})^2}}{4\rho}}$$

where ρ is the mass density. The advantage of this approach is that it does not need too many energy calculations for a given distorted system; it just needs to obtain inter-atomic force constants of the material (all the calculations are performed in the first BZ in the DFPT formalism) once. So, the phonon dispersion curve is useful to obtain the elastic properties of the material. To the best of our knowledge, using this method to calculate elastic constants has rarely been used in other works.

3. Results and discussion

3.1. Phonon spectra

The Born effective charge (Z^*) is the fundamental quantity which monitors the long-range Coulomb interaction that is responsible for the splitting between transverse and longitudinal optical phonon modes. In real systems a dynamic contribution is often superimposed on the static charge (which follows rigidly the displacement of the nuclei in an ideal ionic model) due to the mixed ionic–covalent character of the material. So, the Born effective charge is not equal to its nominal value (+4 for Ti or −2 for O ions in the case of TiO_2). Dielectric tensor elements and Born effective charges for anatase and rutile structures were calculated and are summarized in tables 2–5. These anomalous effective charges

Table 4. Born effective charges calculated for Ti and O atoms in the anatase phase.

Anatase	$Z^{*\text{Ti}}_{\parallel}$	$Z^{*\text{Ti}}_{\perp}$	$Z^{*\text{O}}_{\parallel}$	$Z^{*\text{O}}_{\perp_1}$	$Z^{*\text{O}}_{\perp_2}$
This work (LDA)	5.67	6.66	−2.88	−5.61	−1.19
This work (PW91)	5.76	6.68	−2.89	−5.60	−1.16
Theory[a]	5.71	6.68	−2.86	−5.52	−1.16

[a] Reference [18].

Table 5. Born effective charges calculated for Ti and O atoms in the rutile phase.

Rutile	$Z^{*\text{Ti}}_{\parallel}$	$Z^{*\text{Ti}}_{\perp_1}$	$Z^{*\text{Ti}}_{\perp_2}$	$Z^{*\text{O}}_{\parallel}$	$Z^{*\text{O}}_{\perp_1}$	$Z^{*\text{O}}_{\perp_2}$
This work (LDA)	7.32	5.25	7.27	−3.64	−4.98	−1.40
This work (PW91)	7.52	5.18	7.22	−3.71	−4.88	−1.36
Theory[a]	7.54	5.34	7.34	−3.77	−4.98	−1.36

[a] Reference [12].

have already been discussed concerning the dynamical transfer of charge due to modification of the bond hybridization during the atomic displacement [12, 18]. The Born effective charge tensor associated with a given atom reflects its site symmetry. So, it has three independent components for the oxygen ions in anatase and rutile phases (C_{2v} symmetry), as well as for the titanium ions in the rutile (D_{2h} symmetry) phase. In the anatase structure, the site symmetry of the titanium ions is higher (D_{2d}) and the corresponding Born charge tensor has only two independent components: perpendicular and parallel to the principal tetragonal axis. The Z^* tensor is already diagonal in the conventional Cartesian reference frame of anatase but it is not in the rutile phase and it should be diagonalized to obtain the effective charges. The dielectric tensor elements and Born effective charges calculated in this work are in good agreement with the other *ab initio* reports [12, 18].

In order to obtain the zone-center phonons of the polymorphs, the dynamical matrix should be diagonalized for $q = 0$. By means of factor analysis [36], in the $I4_1amd$ ($P4_2/mnm$) space group for the anatase (rutile) phase, the irreducible representations of optical vibrations are as follows:

$$\text{anatase: } \Gamma_{\text{opt}} = \text{A}_{1\text{g}} + \text{A}_{2\text{u}} + 2\text{B}_{1\text{g}} + \text{B}_{2\text{u}} + 2\text{E}_{\text{g}} + 2\text{E}_{\text{u}},$$

$$\text{rutile: } \Gamma_{\text{opt}} = \text{A}_{1\text{g}} + \text{A}_{2\text{g}} + \text{A}_{2\text{u}} + 2\text{B}_{1\text{u}} + \text{B}_{1\text{g}} + \text{B}_{2\text{g}} + \text{E}_{\text{g}} + 3\text{E}_{\text{u}}.$$

The representations with subscript g are Raman-active and those with u are infrared-active, while the representations with the E symbol are degenerate. The zone-center phonons of the anatase (rutile) phase calculated in this work are presented in table 6 (7) which was compared with some other computational and experimental data. The LDA results are in good agreement with the experimental data (like the other reports), and the PW91 approximation underestimates the measured frequencies, as has already been reported for the rutile structure [13].

There are some special notes about B_{1g}, B_{1u} and A_{2u}(TO) modes in the rutile phase; according to Montanari and Harrison's report [13], B_{1g} is the only mode for which the gradient-corrected functionals (like PW91) overestimate the measured frequencies [13]. However, diagonalizing the

Table 6. Zone-center phonon frequencies of the anatase phase (in cm^{-1}).

Mode (anatase)	This work (LDA)	This work (PW91)	Theory[a]	Exp.[b]	Exp.[c]
E_g	140.8	138.4	145.6	—	144
E_g	164.1	163.8	171.1	—	197
E_u(TO)	243.6	229.7	248.6	262	—
E_u(LO)	340.7	292.1	340.6	366	—
A_{2u}(TO)	351.8	299.7	375.3	367	—
B_{1g}	390.7	357.8	398.4	—	399
E_u(TO)	459.4	400.5	479.9	435	—
B_{1g}	506.5	476.6	518.4	—	519
A_{1g}	528.0	493.0	535.9	—	513
B_{2u}	555.8	521.0	564.6	—	—
E_g	650.4	606.0	662.1	—	639
A_{2u}(LO)	728.8	688.8	743.1	755	—
E_u(LO)	880.0	826.5	892.2	876	—

[a] Reference [18]. [b] Reference [35]. [c] Reference [37].

Table 7. Zone-center phonon frequencies of the rutile phase (in cm^{-1}).

Mode (rutile)	This work (LDA)	This work (PW91)	Theory[a]	Theory[b]	Exp.[c]	Exp.[d]
B_{1u}	111.0	132.8	116.7	117.7	113	—
B_{1g}	131.8	159.8	125.2	132.0	142	143
A_{2u}(TO)	157.5	111.2	176.1	191.3	173	167
E_u(TO)	162.9	111.0	164.8	143.7	189	183
E_u(LO)	357.6	357.0	351.5	352.3	375	373
E_u(TO)	391.5	363.8	391.3	393.0	—	388
B_{1u}	404.2	362.9	407.5	417.3	406	—
A_{2g}	422.2	422.4	415.5	412.7	—	—
E_u(LO)	442.7	430.8	441.7	434.7	429	458
E_g	472.9	433.9	471.5	472.0	445	447
E_u(TO)	497.8	479.7	492.8	498.3	494	500
A_{1g}	622.7	574.5	622.5	615.3	610	612
A_{2u}(LO)	761.3	741.3	769.3	800.7	—	769
E_u(LO)	803.7	754.7	808.4	787.7	—	812
B_{2g}	830.7	776.8	828.0	800.7	825	827

[a] Reference [12]. [b] Reference [17]. [c] Reference [38].
[d] Reference [39, 40].

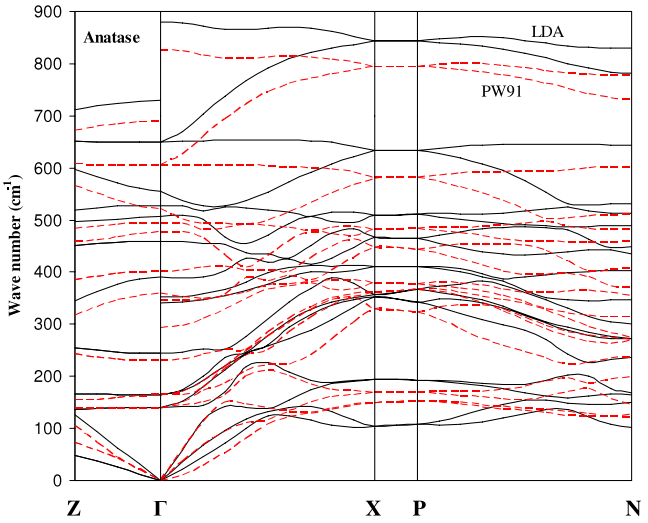

Figure 1. Phonon band structure of the anatase phase within LDA and PW91.

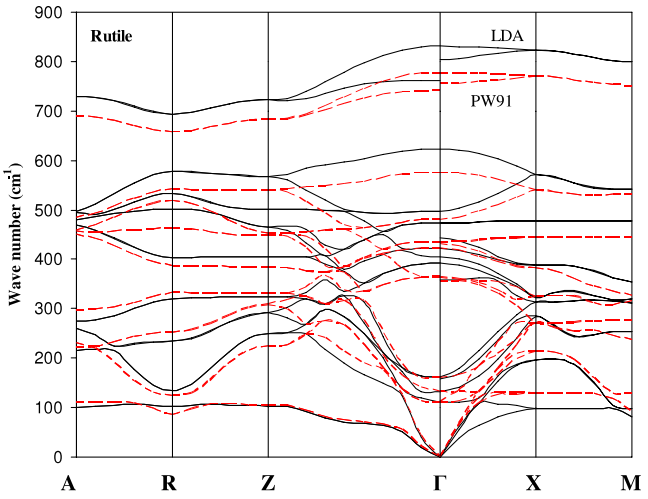

Figure 2. Phonon band structure of the rutile phase within LDA and PW91.

dynamical matrix at the gamma point predicts the same result for B_{1u}. This can be solved by using different acoustic sum rules [41] to diagonalize the dynamical matrix. Using different acoustic sum rules means different ways to impose the translational invariance in the dynamical matrix at zone center. About the A_{2u}(TO) mode, the authors [13] have shown that the PBE functional predicts it is imaginary, which leads to the unstable crystal for a distortion along this ferroelectric mode, in disagreement with all previous observations. According to their results the PW91 functional predicts it to be very slightly positive, underestimating the experimental frequency by almost 100 cm^{-1}. However, our results underestimate the experimental frequency by about 60 cm^{-1}. It should be noted that the instability in the A_{2u}(TO) mode may be observed using different sum rules even in the PW91 approximation. The longitudinal optical modes calculated by means of Born effective charges in this work are also listed in tables 6 and 7.

The phonon band structure was obtained by calculating the phonon frequencies for a set of points on a track passing the high-symmetry points in the first BZ of the anatase and rutile structures within both LDA and PW91 (figures 1 and 2). The LDA results for the anatase phase are compatible with the results of Mikami *et al* [18] and there is no report on the anatase structure using PW91. The only work which has been performed for the rutile phase is [17], which has used the inter-atomic force constants of high-symmetry points in the first BZ within the supercell method to obtain the phonon frequencies for the other wavevectors. Comparing the phonon band structures in the LDA with PW91 for both anatase and rutile structures shows the PW91 bands have been shifted down to low frequencies with respect to the LDA bands. This shows its effect in the heat capacity calculation, which is clear in the calculated phonon density of states in figures 3 and 4, too. We should mention that the effect of PW91 (lowering the frequencies of phonons) is more noticeable at larger wavenumbers in both anatase and rutile phases. There is a gap in the phonon density of states of both polymorphs in the high energy region. The gap in the phonon density of

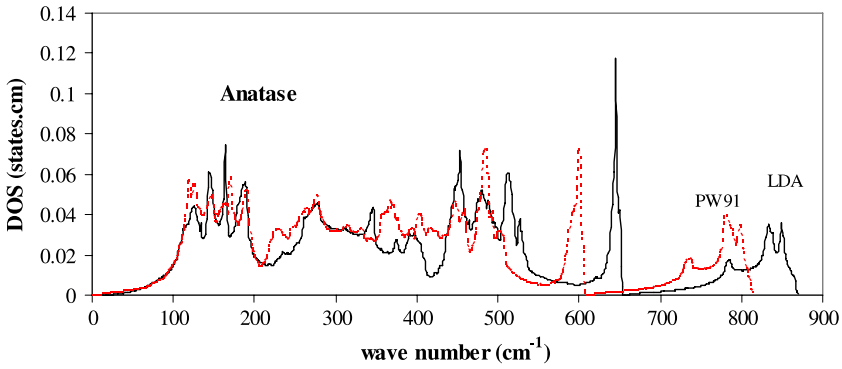

Figure 3. Phonon density of states of the anatase phase within LDA and PW91.

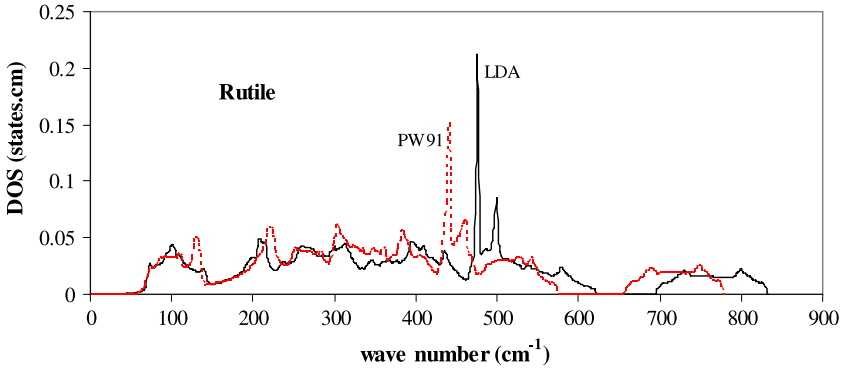

Figure 4. Phonon density of states of the rutile phase within LDA and PW91.

states in rutile is larger than the one in the anatase structure. It seems that is due to the greater ionicity of the rutile structure, which also shows itself in the greater Born effective charges. To examine this, we changed the Born effective charges of the rutile structure to smaller values, which tend to produce a few numbers of states in the gap region. We should note that there are a few numbers of states in the region below 700 cm^{-1} and above the gap in the anatase structure. This is quite similar to the case of the rutile structure, when changing the values of the Born effective charges. To the best of our knowledge there is no report on the phonon density of states for the anatase structure. In the case of the rutile structure, our calculated phonon density of states is quite different even qualitatively than those reported in [17] and [38]. In addition, we should note that the phonon density of states reported in [38] is the frequency distribution presented for a model that has been fitted to the experimental phonon band structure, and the authors claim the model is more or less good [38].

3.2. Heat capacity, Debye temperature and mean sound velocity

Heat capacities of the polymorphs were calculated using

$$\frac{c_v(T)}{k_B} = \sum_p \int_0^\infty d\omega D_p(\omega) \frac{x^2 \exp x}{(\exp x - 1)^2},$$

where $x = \hbar\omega/k_B T$ and p is the number of bands. Since TiO_2 polymorphs are semiconductors, the phonon density of states is the main component in calculation of the heat capacity of materials. The calculated molar heat capacities up to 300 K within both LDA and PW91 were presented in figures 5 and 6. We cannot compare these heat capacities to experiment because all measured heat capacities in the experiment are at a constant pressure. To obtain reasonable values for the heat capacity in a constant volume, we need to know the thermal expansion coefficient, but there are no measured thermal expansion coefficients in the low temperatures for both anatase and rutile structures. It is observed that PW91 leads to larger values of heat capacity in both the anatase and rutile phases (at higher temperatures). The reason seems to be the larger occupations of states with lower phonon frequencies in the PW91 compared with the LDA one. In addition, we know the low frequency states have a more important role in heat capacity. The effect of the calculated phonon density of states shows itself in low temperatures, where x is large. At high temperatures, the heat capacity approaches the asymptotic Dulong–Petit value.

The Debye temperature was calculated (table 8) by a linear fit of c_v with respect to T^3 at very low temperatures ($T < 1$ K). As we know, the Debye temperature shows the stiffness of the material. Therefore, we expect the rutile phase to have a larger Debye temperature than the anatase phase. In addition, the PW91 should reduce the Debye temperature, because it reduces the values of phonon frequencies (including the acoustic modes). It increases the heat capacity and therefore decreases the Debye temperature. As we see, both LDA and

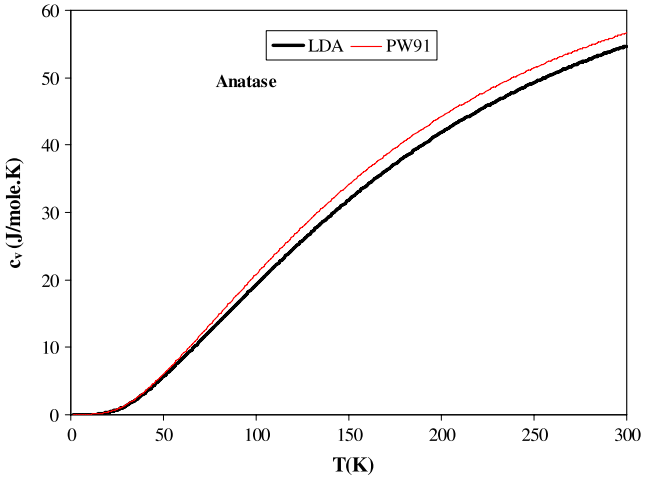

Figure 5. Temperature-dependent calculated molar heat capacity of the anatase phase.

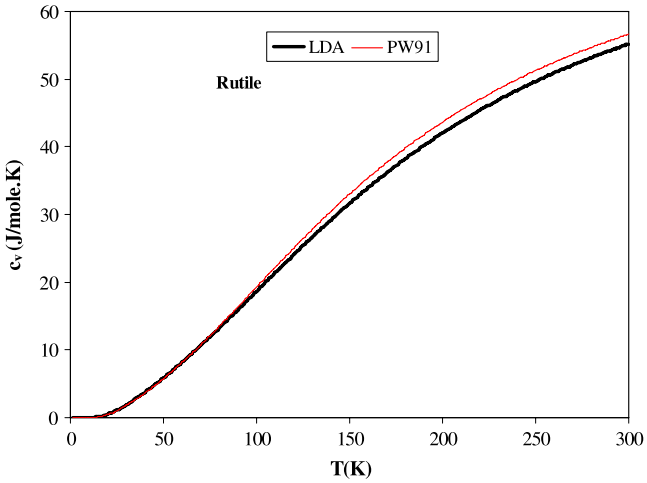

Figure 6. Temperature-dependent calculated molar heat capacity of the rutile phase.

PW91 predict the Debye temperature of the anatase phase to be lower than the rutile phase. On the other hand, PW91 reduces the Debye temperature of the anatase structure, but increases the Debye temperature of the rutile structure. The heat capacity at room temperature, Debye temperature, bulk modulus and its pressure derivative (by fitting the calculated energy-volume data to the Murnaghan equation of state) obtained in the present work, other computational work and the experimental data are listed in table 8. It is observed that the LDA heat capacities at room temperature for both anatase and rutile phases are in better agreement with the experiments compared to the PW91 functional. However, PW91 leads to a more comparable bulk modulus with respect to the experiment and [3]. It should be considered that the bulk modulus reported in [3] is the arithmetic average of the Reuss and Voigt [47] values, calculated using theoretical elastic constants. On the other hand, according to the work of Glassford and Chelikowsky [48] to investigate the effect of temperature on B_0 in the rutile structure, if someone extrapolates B_0 quadratically to absolute zero temperature (at which our calculations were performed)

Table 8. Calculated Debye temperature, mean sound velocity, molar heat capacity at room temperature, bulk modulus and pressure derivative of bulk modulus for anatase and rutile phases.

		Θ_D (K)	c_v (J mol^{-1} K^{-1}) (RT)	B_0 (GPa)	B_0'
Anatase	LDA[a]	881	54.53	187	5.63
	PW91[a]	511	56.42	173	2.73
	Theory	—	—	174[b]	—
	Exp.	—	54.62[c]	179[d]–178[e]	4.5[d]
Rutile	LDA[a]	987	54.99	241	7.95
	PW91[a]	1270	56.43	201	4.87
	Theory	815[f]	—	204[b]	—
	Exp.	778[g]	54.13[c]	211[h]	6.5[h]

[a] This work. [b] Reference [3]. [c] Reference [45]. [d] Reference [42]. [e] Reference [46]. [f] Reference [17]. [g] Reference [43] (see footnote 4). [h] Reference [44].

using the low temperature elastic constant measurements [49], they find the value 239 GPa, which is in excellent agreement with the LDA result.

3.3. Elastic constants

Using the inter-atomic force constants, the phonon frequencies of the points near the gamma point (with components equal to $\frac{1}{10}\vec{b}_i$, $\frac{5}{100}\vec{b}_i$ and $\frac{25}{1000}\vec{b}_i$ for all the symmetry directions) in the symmetry directions of the anatase and rutile phases were obtained. Then, the elastic constants of the polymorphs were calculated by linear fit to the acoustic branches. Our calculated elastic constants, the data from the stress–strain method [3] and the experimental values are presented in table 8. The elastic constants of [3] have been calculated by linear fit to the calculated stress as a function of strain, using the PBE functional [15]. At first glance, 33 Ryd seems to be sufficient for energy cutoff in the wavefunctions, especially in ultrasoft pseudopotentials. This cutoff leads to a reliable heat capacity at room temperature for both anatase and rutile structures, but it is not enough to obtain the right acoustic branches of the phonon band structure and, as a consequence, the elastic constants. The calculated elastic constants with 33 Ryd energy cutoff are not in agreement with the experiment [49, 50]. So, we have tested the fully optimized structures with larger energy cutoff equal to 44 Ryd in wavefunctions (880 Ryd in charge density) to investigate the descents of the acoustic branches. It considerably improves the results as presented in tables 9 and 10.

We focused our attention on calculating elastic constants with higher energy cutoff. The PW91 result for the anatase phase has improved C_{11}. The other coefficients are quite similar to the LDA results and are in good agreement with the stress–strain method results [3]. In the case of the rutile phase, PW91 improves the C_{12}, C_{13}, C_{33} and C_{66} coefficients considerably with respect to the LDA results, which become in good agreement with the stress–strain method data and the experiment. It is noticeable that, according to the experimental measurements for the rutile structure [49, 50], C_{11}, C_{12}, C_{13}, C_{33}, C_{44} and C_{66} increase at lower temperatures, which rise

Table 9. Elastic constants (in GPa) of anatase and rutile phases calculated with 33 Ryd energy cutoff. (Note: RT means room temperature.)

		C_{11}	C_{12}	C_{13}	C_{33}	C_{44}	C_{66}
Anatase	LDA[a]	398	157	156	200	33	58
	PW91[a]	337	104	183	97	87	91
	Theory[b]	320	151	143	190	54	60
	Exp.	—	—	—	—	—	—
Rutile	LDA[a]	316	216	211	569	113	263
	PW91[a]	377	83	110	583	136	327
	Theory[b]	278	153	149	479	115	214
	Exp.[c] (RT)	271	177	149	484	124	194
	Exp.	289[d]	197[d]	159[e]	508[e]	128[e]	227[d]

[a] This work. [b] Reference [3]. [c] Reference [49, 50].
[d] Measured at 4 K [50]. [e] Measured at 80 K [49];

Table 10. Elastic constants (in GPa) of anatase and rutile phases calculated with 44 Ryd energy cutoff. (Note: RT means room temperature.)

		C_{11}	C_{12}	C_{13}	C_{33}	C_{44}	C_{66}
Anatase	LDA[a]	399	156	152	203	34	60
	PW91[a]	333	143	140	198	39	57
	Theory[b]	320	151	143	190	54	60
	Exp.	—	—	—	—	—	—
Rutile	LDA[a]	303	222	205	561	113	251
	PW91[a]	269	189	166	506	105	217
	Theory[b]	278	153	149	479	115	214
	Exp.[c] (RT)	271	177	149	484	124	194
	Exp.	289[d]	197[d]	159[e]	508[e]	128[e]	227[d]

[a] This work. [b] Reference [3]. [c] Reference [49, 50].
[d] Measured at 4 K [50]. [e] Measured at 80 K [49].

to values in better agreement with our results. Apart from the elastic constants, this approach helps us to investigate the accuracy of the calculation of the phonon band structure in different symmetry directions of the crystals.

Using the elastic constants of the polymorphs, we are able to calculate the polycrystalline isotropic shear modulus (G_{VRH}) and bulk modulus (B_{VRH}) by the arithmetic average of Reuss and Voigt values [47]. The interesting quantity which was calculated is the mean sound velocity:

$$v_{\mathrm{m}} = \left[\frac{1}{3}\left(\frac{2}{v_s^3} + \frac{1}{v_l^3}\right)\right]^{-\frac{1}{3}},$$

$$v_s = \sqrt{\frac{G_{\mathrm{VRH}}}{\rho}}, \qquad v_l = \sqrt{\frac{(B_{\mathrm{VRH}} + \frac{4}{3}G_{\mathrm{VRH}})}{\rho}}.$$

This is the sound velocity averaged over all directions and acoustic branches in the crystal. Considering a polycrystalline aggregate as a set of single crystals with random orientations, the averaged sound velocity over all directions of a single crystal should play the role of sound velocity in a real polycrystalline material. The Debye temperature of the polymorphs was calculated by the mean sound velocity:

$$\Theta_{\mathrm{D}} = \frac{\hbar v_{\mathrm{m}}}{k_{\mathrm{B}}}(6\pi^2 n)^{\frac{1}{3}}$$

where $n = \frac{\text{number of atoms in the unit cell}}{\text{volume of the unit cell}}$. The results for both polymorphs in the LDA and PW91 are listed in table 11. The

Table 11. Shear modulus, bulk modulus, mean sound velocity and Debye temperature of anatase and rutile TiO_2 structures calculated with 44 Ryd energy cutoff.

		G_{VRH} (GPa)	B_{VRH} (GPa)	v_{m} (m s^{-1})	Θ_{D} (K)
Anatase	LDA	55	201	4140	557
	PW91	53	183	4181	552
Rutile	LDA	112	262	5594	775
	PW91	104	225	5546	755

Debye temperature for the rutile structure (especially in the case of LDA) is in good agreement with the experimental data [43][4]. The Debye temperature of rutile is larger than the one for anatase, and the values obtained by PW91 are smaller than LDA, as we expect.

4. Conclusions

Dynamical properties of two polymorphs of TiO_2 including phonon band structure and density of states were studied by first-principles calculations based on DFPT and also considering the exchange–correlation interaction in both LDA and PW91. The shift in the phonon band structure (and density of states) to lower frequencies was observed in the case of PW91 with respect to the LDA results. This leads to relatively larger values for the corresponding calculated heat capacity. The elastic constants were obtained by a linear fit to the acoustic branches of the phonon band structure in symmetry directions. It was observed that, in order to obtain more exact elastic constants, we should use quite large energy cutoffs for the wavefunction (and, as a consequence, charge density) expansions. In this case, the PW91 results were in good agreement with the experimental data, where the difference between LDA and PW91 was more noticeable in the case of the rutile phase. The isotropic bulk and shear modulus, mean sound velocity and Debye temperature of the polymorphs were obtained using the elastic constants, which are in good agreement with the experimental data. The Debye temperature and the heat capacity at room temperature of polymorphs in the LDA were better than the PW91. The calculated Born effective charges and dielectric tensor elements with the LDA and PW91 were about the same and in agreement with the other computational works.

Acknowledgments

The partial financial support by the research council of the University of Tehran is acknowledged. The scientific support of the Abdus Salam International Center for Theoretical Physics (ICTP), technical support of the Computational Nanotechnology Supercomputing Center at the Institute for

[4] See also Wu and Sladek [43] which has reported the calorimetric Debye temperature at low temperatures and calculated the Debye temperature of rutile using different methods such as VRHG (at room temperature plus using the elastic constants at low temperature), BBH, BV and also the rigorous value which was calculated using the mean sound velocity obtained by averaging over 400 propagation directions 4.5° apart in one of the eight quadrants of the crystal.

Research in Fundamental Sciences (IPM), S Jadidi, S Bayegan, S M Vaez Allaei and M F Miri are acknowledged. Scientific discussions with S Baroni are acknowledged.

References

[1] McSkimin H J 1961 *J. Acoust. Soc. Am.* **33** 12
[2] Damzen M J 2003 *Stimulated Brillouin Scattering, Fundamentals and Application* (Bristol, MA: Institute of Physics Publishing)
[3] Iuga M, Steinle-Neumann G and Meinhardt J 2007 *Eur. Phys. J.* B **58** 127
[4] Kameli P, Salamati H, Eshraghi M and Mohammadizadeh M R 2005 *J. Appl. Phys.* **98** 043908
Ashkarran A A and Mohammadizadeh M R 2008 *Mater. Res. Bull.* **43** 522
Ashkarran A A and Mohammadizadeh M R 2007 *Eur. Phys. J. Appl. Phys.* **40** 155
Pourmand M and Mohammadizadeh M R 2008 *Curr. Nanosci.* **4** 151 and references therein
[5] Muscat J, Swamy V and Harrison N M 2002 *Phys. Rev.* B **65** 224112
Mattesini M, de Almeida J S, Dubrovinsky L, Dubrovinskaia N, Johansson B and Ahuja R 2004 *Phys. Rev.* B **70** 212101
Swamy V and Muddle B C 2007 *Phys. Rev. Lett.* **98** 035502
Dewhurst J K and Lowther J E 2001 *Phys. Rev.* B **64** 014104
[6] Jones R O and Gunnarsson O 1989 *Rev. Mod. Phys.* **61** 689
[7] Ghanbarian V and Mohammadizadeh M R 2008 *Phys. Rev.* B **78** 144505
Ghanbarian V and Mohammadizadeh M R 2008 *Eur. Phys. J.* B **61** 309
Ghanbarian V and Mohammadizadeh M R 2006 *Phys. Status Solidi* c **3** 3122
[8] Anisimov V I, Korotin M A, Nekrasov I A and Mylnikova A S 2005 arXiv:con-mat/0503625 v1
[9] Wang Y and Doren D J 2005 *Solid State Commun.* **136** 142
[10] Janisch R and Spaldin N A 2006 *Phys. Rev.* B **73** 035201
[11] Lee C and Gonze X 1994 *Phys. Rev.* B **49** 14730
[12] Lee C, Ghosez P and Gonze X 1994 *Phys. Rev.* B **50** 13379
[13] Montanari B and Harrison N M 2002 *Chem. Phys. Lett.* **364** 528
[14] Ceperley D M and Alder B J 1980 *Phys. Rev. Lett.* **45** 566
Perdew J P and Zunger A 1981 *Phys. Rev.* B **23** 5048
[15] Perdew J P, Burke K and Ernzerhof M 1996 *Phys. Rev. Lett.* **77** 3865
[16] Perdew J P 1991 *Electronic Structure of Solids* vol 91, ed P Ziesche and H Eschrig (Berlin: Akademie Verlag) p 11
[17] Sikora R 2005 *J. Phys. Chem. Solids* **66** 1069
[18] Mikami M, Nakamura S, Kitao O and Arakawa H 2002 *Phys. Rev.* B **66** 155213
[19] Gürel T and Eryigit R 2006 *Phys. Rev.* B **74** 014302
[20] Shi S, Ke X, Ouyang C, Zhang H, Ding H, Tang Y, Zhou W, Li P, Lei M and Tang W 2009 *J. Power Sources* **194** 830
[21] Savrasov S Y and Kotliar G 2003 *Phys. Rev. Lett.* **90** 056401
[22] Pisani L and Valenti R 2005 *Phys. Rev.* B **71** 180409(R)
[23] Goffinet M, Hermet P, Bilc D I and Ghosez Ph 2009 *Phys. Rev.* B **79** 014403
[24] Lazzeri M, Attaccalite C, Wirtz L and Mauri F 2008 *Phys. Rev.* B **78** 081406(R)
[25] Giannozzi P, Baroni S, Bonini N, Calandra M, Car R, Cavazzoni C, Ceresoli D, Chiarotti G L, Cococcioni M, Dabo I, Corso A D, de Gironcoli S, Fabris S, Fratesi G, Gebauer R, Gerstmann U, Gougoussis C, Kokalj A, Lazzeri M, Martin-Samos L, Marzari N, Mauri F, Mazzarello R, Paolini S, Pasquarello A, Paulatto L, Sbraccia C, Scandolo S, Sclauzero G, Seitsonen A P, Smogunov A, Umari P and Wentzcovitch R M 2009 *J. Phys.: Condens. Matter* **21** 395502
[26] Giannozzi P, de Gironcoli S, Pavone P and Baroni S 1991 *Phys. Rev.* B **43** 7231
[27] Baroni S, de Gironcoli S, Dal Corso A and Giannozzi P 2001 *Rev. Mod. Phys.* **73** 515
[28] Gonze X and Lee C 1997 *Phys. Rev.* B **55** 10355
[29] Howard C, Sabine T M and Dickson F 1991 *Acta Crystallogr.* B **47** 462
[30] Akbarzadeh H and Mohammadizadeh M R 1997 *Comput. Mater. Sci.* **8** 335
[31] Vanderbilt D 1990 *Phys. Rev.* B **41** 7892
[32] Monkhorst H and Pack J 1976 *Phys. Rev.* B **13** 5188
[33] Lazzeri M, Vittadini A and Selloni A 2001 *Phys. Rev.* B **63** 155409
[34] Auld B 1973 *Acoustic Fields and Waves in Solids* vol 1 (New York: Wiley)
[35] Gonzalez R J, Zallen R and Berger H 1997 *Phys. Rev.* B **55** 7014
[36] Fateley W G, Dollish F R, McDevitt N and Bentley F F 1972 *Infrared and Raman Selection Rules for Molecular and Lattice Vibrations: the Correlation Method* (New York: Wiley)
[37] Ohsaka T, Izumi F and Fujiki Y 1978 *J. Raman Spectrosc.* **7** 321
[38] Traylor J G, Smith H G, Nicklow R M and Wilkinson M K 1971 *Phys. Rev.* B **3** 3457
[39] Porto S P S, Fleury P A and Damen T C 1967 *Phys. Rev.* **154** 522
[40] Eagles D M 1964 *J. Phys. Chem. Solids* **25** 1243
[41] Pick R M, Cohen M H and Martin R M 1970 *Phys. Rev.* B **1** 910
[42] Arlt T, Bermejo M, Blanco M A, Gerward L, Jiang J Z, Olsen J S and Recio J M 2000 *Phys. Rev.* B **61** 14414
[43] Sandin T R and Keesom P H 1969 *Phys. Rev.* **177** 1370
Wu A Y and Sladek R J 1982 *Phys. Rev.* B **25** 5230
[44] Gerward L and Olsen J S 1997 *J. Appl. Crystallogr.* **30** 259
[45] Howard Shomate C 1947 *J. Am. Chem. Soc.* **69** 218
[46] Swamy V and Dubrovinsky L S 2001 *J. Phys. Chem. Solids* **62** 673
[47] Reuss A 1929 *Z. Angew. Math. Mech.* **9** 49
Voigt W 1889 *Wied. Ann.* **38** 573
[48] Glassford K M and Chelikowsky J R 1992 *Phys. Rev.* B **46** 1284
[49] Fritz I J 1974 *J. Phys. Chem. Solids* **35** 817
[50] Manghnani M H, Fisher E S and Brower W S Jr 1972 *J. Phys. Chem. Solids* **33** 2149